PAPER

Check for updates

A comparison of *para*, *meta*, and *ortho*-carborane centred non-fullerene acceptors for organic solar cells†

Filip Aniés, [ID] [a] Francesco Furlan, [a] Zhuoran Qiao, [a] Valentina Pirela, [b] Matthew Bidwell, [ID] [a] Martina Rimmele, [ID] [a] Jaime Martín, [ID] [bcd] Nicola Gasparini [ID] [a] and Martin Heeney [ID] *[ae]

We report the first examples of carborane-containing non-fullerene acceptors (NFAs), and their use in organic photovoltaic (OPV) devices. NFAs employing an A–D–A'–D–A type design centred around a central electron withdrawing carborane unit (A'), using either *para*, *meta*, or *ortho*-carborane isomers are reported. We demonstrate that the nature of the isomer has a major impact on device performance, despite minor differences in optoelectronic and morphological properties, with the use of *ortho*-carborane resulting in the highest device efficiencies. We further show that end-group fluorination is an efficient strategy to modulate energy levels and improve device performance of such NFAs.

Introduction

Carboranes are a peculiar class of atom clusters: consisting of hydrogen substituted carbon and boron atoms, they are held together by delocalised electrons in a three-centre two-electron fashion, sometimes referred to as "3-D aromaticity".[1] This unique structure results in chemically and thermally very stable compounds – properties which can sometimes be transposed onto other materials and compounds by chemically incorporating carborane species.[2–4] Due to their high boron density, and the high neutron cross-section of ^{10}B, carboranes may also be particularly suitable for neutron capture applications, such as neutron detection or boron neutron capture therapy to treat cancer, in addition to other biomedical applications.[5–9]

In recent years, attention has been drawn towards the use of carboranes in various conjugated chemical scaffolds. Typically, such species contain one of the three *para*, *meta*, and *ortho* (*p*, *m*, *o*) isomers of the $C_2B_{10}H_{12}$ icosahedron, with conjugated substituents at one or both of the carbon atoms. Depending on the substituent groups, such species may cover a wide range of potential applications. Most prominent are perhaps light-emitting compounds and applications, partly driven by interesting aggregation induced emission (AIE) properties in many *o*-carborane-containing species.[10–17] Such properties can be finely tuned through the choice of conjugated substituent groups, and may result in responsivity to external factors such as thermal or mechanical stimuli, or exposure to solvent vapours.[18–27] Emissive carborane species have also been demonstrated as the photoactive component in organic light emitting diodes on several occasions.[28–32]

Examples of emissive carborane-containing species also include a number of conjugated polymers, with emissive properties depending on the selection of carborane isomer and substituent site, and a certain tuneability based on the selection of conjugated co-monomers.[33–36] Different designs have been explored regarding the incorporation of carborane into polymeric species, including the use of carborane in the polymer backbone, fusing carborane into conjugated monomers, and attaching carborane onto solubilising side chains.[37–43] To further explore potential applications of carborane-containing conjugated materials, we have previously shown that such polymers may be used as the semiconductor layer in organic field-effect transistors: polymers with fused benzocarborane and benzocarboranodithiophene monomers, as well as polythiophenes with pendant carboranes, exhibited p-type behaviour, whilst P(NDI2OD-T2)-inspired polymers with carborane in the backbone exhibited n-type behaviour.[38–41] Similar devices have also been made with a phthalocyanine unit linked to a carborane moiety.[44]

[a] Department of Chemistry and Centre for Processable Electronics, Imperial College London, Molecular Sciences Research Hub, 80 Wood Lane, London, W12 0BZ, UK

[b] POLYMAT, University of the Basque Country UPV/EHU Av. de Tolosa 72, Donostia-San Sebastián, Spain

[c] Universidade da Coruña, Grupo de Polímeros, Centro de Investigacións Tecnolóxicas (CIT), Esteiro, 15471, Ferrol, Spain

[d] Ikerbasque, Basque Foundation for Science, 48013, Bilbao, Spain

[e] KAUST Solar Center (KSC), Physical Science and Engineering Division (PSE), King Abdullah University of Science and Technology (KAUST), Thuwal, 23955-6900, Saudi Arabia. E-mail: martin.heeney@kaust.edu.sa

This journal is © The Royal Society of Chemistry 2023

J. Mater. Chem. C, 2023, 11, 3989–3996 | 3989

Furthermore, the aforementioned polythiophene and NDI based polymers constitute, to the best of our knowledge, the only two examples where carborane-containing materials have been used in organic photovoltaic (OPV) devices. Carborane-containing polythiophenes reached a maximum power conversion efficiency (PCE) of 2.0% in devices employing PCBM as the acceptor material, whilst carborane-containing NDI polymers reached 1.8% with PM6 as the donor material.[40,41] Other notable materials which have been used in the context of photovoltaic technologies include o-carborane derivatives as electron and hole transport layers in perovskite solar cells, bis(dicarbollide) species as redox shuttles in dye-sensitised solar cells (DSSCs), and o-carborane linked phthalocyanines as photosensitisers in DSSCs.[45–49]
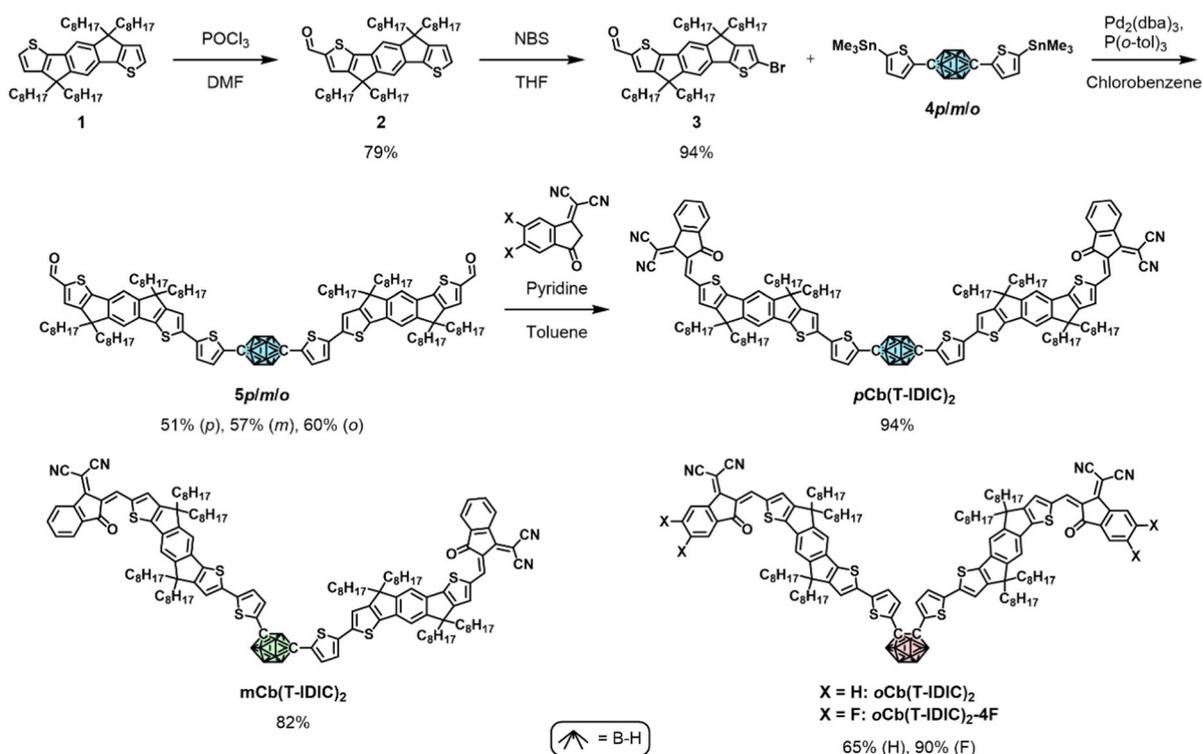
In this work, we further explore design strategies of carborane-containing materials in OPVs. With a series of four carborane-centred conjugated small molecules, featuring each of the three icosahedral isomers as well as one fluorinated species, we present the first examples of carborane-containing non-fullerene acceptors (NFAs). Device data confirms that this is indeed a suitable strategy towards carborane-containing OPV materials, with the fluorinated species exhibiting PCE values above 5% – more than double the previous record for carborane-containing OPV materials. By comparing the different NFAs, it is clear that the choice of carborane isomer has a great impact on device performance, with o-carborane exhibiting the best performance.

Results and discussion

Synthesis and molecular design

We based the design of our NFAs on the principles of alternating electron accepting and donating moieties. The acceptor–donor–acceptor (A–D–A) molecular architecture has proven hugely successful and has become a leading design strategy towards high-performing NFAs, encompassing a central electron rich core flanked by two electron deficient end-groups.[50–54] The indaceno-dithiophene (IDT) core is one of the most widely employed electron donating moieties for such compounds.[55] Commonly occurring examples include IDIC, IDTBR, and IEIC and their many derivatives, as well as ITIC employing a structurally similar indacenodithienothiophene (IDTT) core.[56–61] Of those examples IDIC, ITIC, and IEIC also feature the 2-(3-oxo-2,3-dihydroinden-1-ylidene)-malononitrile (INCN) end-group. Recently, a number of A–D–A′–D–A and A–D–D′–D–A type NFAs have been reported where electron rich IDT and electron deficient INCN moieties are centred around a third component, of either electron rich (D′) or electron deficient (A′) character.[62–67] Efficiencies of OPVs employing such materials have been reported between 2.7 and 11.9%, where the PBDB-T polymer was used as the electron donating species in the highest performing devices.[62] Overall, the NFAs centred around an electron deficient moiety have proven more successful than those with an electron rich moiety.

Inspired by these designs, we envisioned an A–D–A′–D–A type NFA centred around an inductively electron withdrawing

Scheme 1 Synthetic routes to the featured NFAs, and their molecular structures. For each NFA, stannylated compounds of the respective carborane isomer (coloured) were used.

3990 | J. Mater. Chem. C, 2023, **11**, 3989–3996

This journal is © The Royal Society of Chemistry 2023

carborane. Furthermore, the use of different carborane isomers should reveal their impact on the overall performance of the material, as well as significantly influence the molecular shape of the resulting NFA, from linear (with *p*-carborane) to clam-shell (with *o*-carborane). Therefore, we synthesised the three isomeric NFAs *p*Cb(T-IDIC)$_2$, *m*Cb(T-IDIC)$_2$, and *o*Cb(T-IDIC)$_2$. Based on initial device performance, we also prepared a version containing a fluorinated INCN end-group, to fine tune the energetics of the frontier molecular orbitals (FMOs).

The synthetic route to the target NFAs is outlined in Scheme 1. Starting from alkylated IDT (**1**), treatment with phosphorous oxychloride in the presence of DMF afforded the mono-aldehyde (**2**) in 79% yield following chromatographic purification. Subsequent treatment with *N*-bromosuccinimide afforded the key intermediate (**3**) in near-quantitative yield.[62,68] Intermediate **3** was reacted under Stille coupling conditions with a stannylated di(5-(trimethylstannyl)thiophen-2-yl)carborane of each of the three carborane isomers (**4**). Following purification by recycling preparative gel permeation chromatography, the three isomers (**5**) were isolated in similar yields (50–60%). The stannylated carborane species (**4**) were prepared as we have previously reported.[41] Briefly, carborane was substituted with thiophene on the C positions through Ullmann (*para*, *meta*) or Kumada (*ortho*) type reactions, followed by deprotonation of the thiophene substituents with *n*-BuLi and subsequent stannylation using trimethyltin chloride. Finally, the INCN end-group, or the fluorinated equivalent, was reacted with the resulting dialdehyde *via* a Knoevenagel reaction in high yields (65–94%), in accordance with literature procedures.[58,62]

The structure of all final compounds was confirmed with a combination of ^{1}H, ^{11}B and ^{13}C NMR spectroscopy, together with mass spectrometry. Thermal gravimetric analyses (TGA) of the resulting species were nearly identical (Fig. S1, ESI†), proving high thermal stabilities, with a 5% loss of mass at $T_{\mathrm{d,5\%}} = 332$ °C, and a second degradation step at 411 °C.

Optoelectronic properties

To gain insight into the optical properties of the synthesised materials, absorption and photoluminescence spectroscopy was performed. As seen in Fig. 1a, absorption and emission properties of the four materials exhibited near identical behaviours in dichloromethane solution. As summarised in Table 1, absorption and emission maxima are slightly blue-shifted when progressing from the *para* to the *meta* to the *ortho* species, although they remain within a range of 10 and 15 nm for absorption and emission wavelengths respectively. Fluorination of the *ortho* species, however, causes a red-shift in absorption of 12 nm, and a red-shift in emission of 13 nm. Time-dependent density functional theory (TD-DFT) reveals that the excitations which give rise to the main absorption peaks of *p*Cb(T-IDIC)$_2$ and *m*Cb(T-IDIC)$_2$ originates from the HOMO → LUMO (75–80%) and HOMO−1 → LUMO+1 (19–24%) transitions (Fig. S2a and b, ESI†). Whilst this excited state makes a significant contribution to the main absorption peak also in *o*Cb(T-IDIC)$_2$ and *o*Cb(T-IDIC)$_2$-4F, the main contribution comes from a different excited state with almost twice
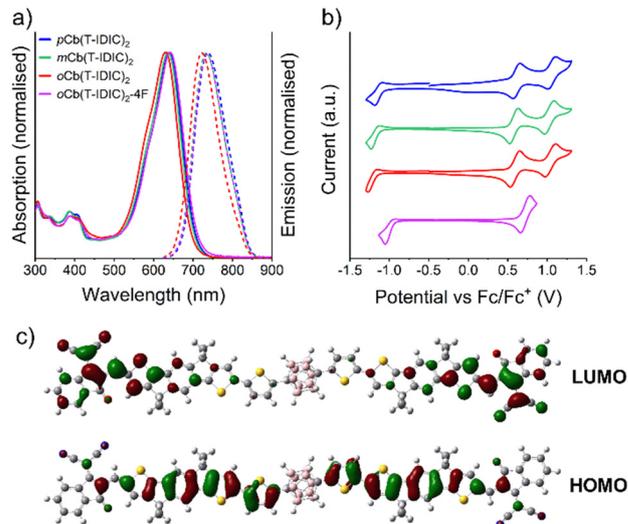

Fig. 1 (a) Absorption and emission spectra of NFA solutions in DCM. (b) Cyclic voltammograms of NFAs, scanning at 0.1 V s^{-1} and using the Fc/Fc$^+$ couple as an internal reference. (c) Frontier molecular orbitals of *p*Cb(T-IDIC)$_2$, as predicted with DFT (B3LYP/6-311G**).

Table 1 Optoelectronic parameters of featured NFAs. $\lambda_{\mathrm{ex}} = 600$ nm. Cyclic voltammetry is referenced against Fc/Fc$^+$

	$\lambda_{\mathrm{abs,max}}$ (nm)	$\lambda_{\mathrm{abs,ons}}$ (nm)	$\lambda_{\mathrm{PL,max}}$ (nm)	Stokes shift (cm^{-1})	$E_{\frac{1}{2},\mathrm{red}}$ (V)	$E_{\frac{1}{2},\mathrm{ox1}}$ (V)	$E_{\frac{1}{2},\mathrm{ox2}}$ (V)
*p*Cb(T-IDIC)$_2$	640	708	737	2056	−1.13	0.61	1.06
*m*Cb(T-IDIC)$_2$	636	702	733	2080	−1.18	0.58	1.03
*o*Cb(T-IDIC)$_2$	630	698	722	2023	−1.21	0.59	1.04
*o*Cb(T-IDIC)$_2$-4F	642	709	735	1971	−1.00	0.72	—

the oscillation strength, resulting from HOMO−1 → LUMO (87%) and HOMO → LUMO+1 (12%) transitions (Fig. S2c and d, ESI†).

To investigate the electrochemical properties of the materials, cyclic voltammetry (CV) was performed, using the ferrocene/ferrocenium (Fc/Fc$^+$) couple as an internal reference, as depicted in Fig. 1b and summarised in Table 1. Once again, the isomeric differences of the molecular structures did not significantly impact the electrochemical properties of the species. *p*, *m*, and *o*Cb(T-IDIC)$_2$ all exhibited very similar voltammograms: one reduction peak around −1.17 V, and two reversible oxidation peaks around 0.59 and 1.04 V. Fluorination of *o*Cb(T-IDIC)$_2$-4F, however, resulted in a shift of the reduction and oxidation peaks towards higher potentials, by up to 0.21 V. The second oxidation peak of *o*Cb(T-IDIC)$_2$-4F was not reversible, and oxidation at high potentials seemed to cause film degradation, and thus the analysis was limited to the first oxidation peak.

Redox potentials acquired through CV are commonly used to estimate the HOMO and LUMO energy levels of organic semiconductors, using Fc/Fc$^+$ = 4.8 V as an electrochemical reference. As seen in Table 2, HOMO and LUMO levels are estimated around −5.39 and −3.63 eV for *p*, *m*, and

This journal is © The Royal Society of Chemistry 2023

J. Mater. Chem. C, 2023, **11**, 3989–3996 | **3991**

Table 2 Molecular energy levels and bandgaps derived from CV, DFT, and UV-vis data

	HOMO (eV)		LUMO (eV)		E_g (eV)		
	CV	DFT	CV	DFT	CV	DFT	UV-Vis
pCb(T-IDIC)$_2$	−5.41	−5.58	−3.67	−3.36	1.74	2.22	1.75
mCb(T-IDIC)$_2$	−5.38	−5.62	−3.62	−3.38	1.76	2.24	1.77
oCb(T-IDIC)$_2$	−5.39	−5.73	−3.59	−3.45	1.80	2.28	1.78
oCb(T-IDIC)$_2$-4F	−5.52	−5.84	−3.80	−3.61	1.72	2.23	1.75

oCb(T-IDIC)$_2$. oCb(T-IDIC)$_2$-4F FMOs are estimated at slightly lower at −5.52 and −3.80 eV, reflecting the very high electronegativity of the fluorine atoms. It can also be seen that the energy differences between the estimated HOMOs and LUMOs correspond very well to the optical bandgap, as obtained from the absorption onset, at around 1.76 eV. The general trend is a very slight bandgap increase when moving from the *para* to the *meta* to the *ortho* isomer. The fluorinated oCb(T-IDIC)$_2$-4F slightly narrows the bandgap, as was also indicated by a red-shift in the absorption spectrum compared to its non-fluorinated equivalent oCb(T-IDIC)$_2$.

Density functional theory (DFT) optimisation was used to predict the structure of the synthesised NFAs, as well as the electron density of their respective HOMOs and LUMOs, as depicted in Fig. 1c and Fig. S3 (ESI†). As is typical for A–D–A type NFAs, and by extension A–D–A′–D–A NFAs, the HOMO was primarily located on the electron-rich IDT moiety, whilst the LUMO was mainly located around the electron-deficient INCN moiety. Notably, no electron density was observed around the

carborane moiety in either FMO. Whilst this is typical for p- and m-carborane species, it stands in contrast to many previously reported aryl substituted o-carborane species, where intramolecular charge transfer (ICT) may result in a significant portion of the LUMO being located on the carborane cage.[69,70] Such a mechanism is typically accompanied by AIE behaviour, which was not observed for any of the NFAs presented herein. A plausible explanation for the absence of ICT is the presence of the strongly electron withdrawing INCN end-groups preventing electron transfer to the carborane cage. Accordingly, DFT calculations predict a partial ICT between the IDT and INCN moieties instead, as mentioned above. This is similar to previous observations where strongly electron withdrawing moieties are present in the conjugated backbone.[41]

Overall, DFT calculations predict deeper HOMOs and shallower LUMOs compared to estimates derived from CV (Table 2), resulting in considerably wider bandgaps around 2.24 eV. Once again, this behaviour has been observed in the past, and a common explanation for this discrepancy is the solvation effect in electrochemical measurements, whilst DFT calculations typically refer to a single isolated species in vacuum.[71]

Morphology comparison of isomers

To investigate how isomer variation impacts thin-film morphology, atomic force microscopy (AFM) was employed. Fig. 2a displays the resulting surface topography images of p, m, and oCb(T-IDIC)$_2$. As can be seen, film surfaces of pristine NFAs were homogenous and overall featureless, with no noticeable

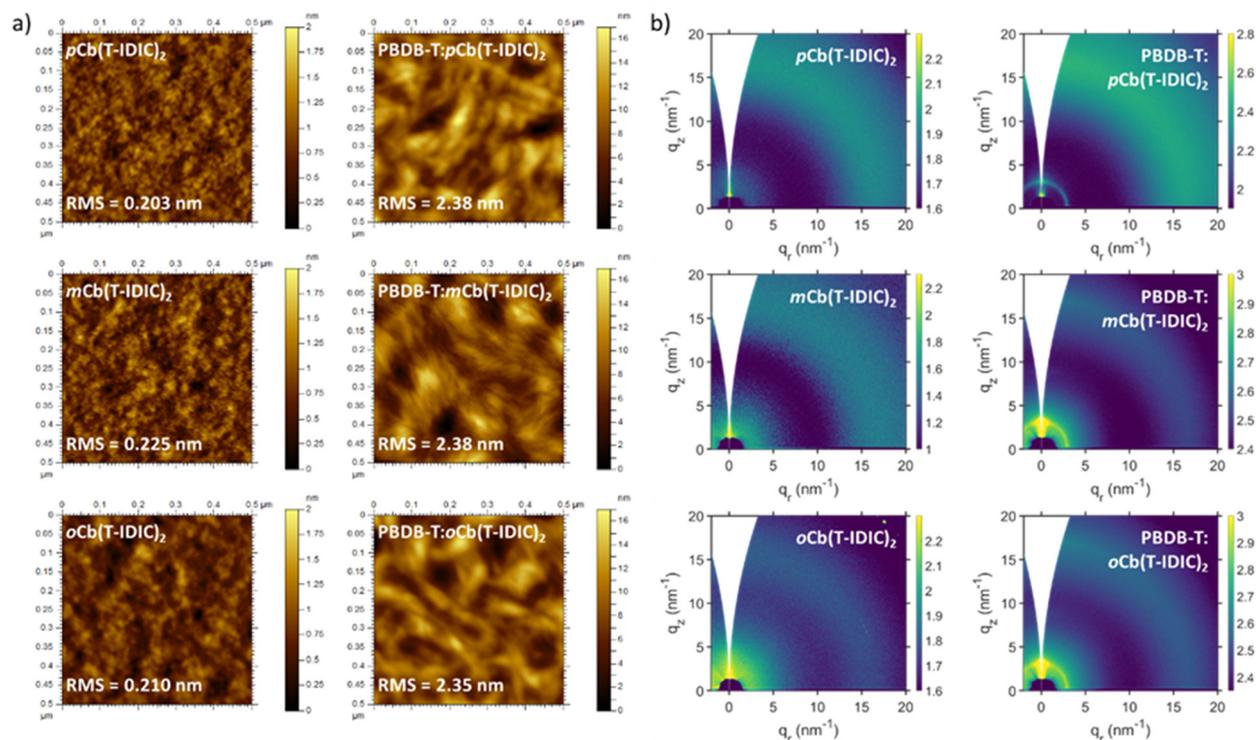**Fig. 2** (a) AFM images and (b) GIWAXS scans of pristine and polymer blend thin-films of NFAs featuring each of the three carborane isomers.

3992 | *J. Mater. Chem. C*, 2023, **11**, 3989–3996

This journal is © The Royal Society of Chemistry 2023

differences between materials. All films were smooth with low root mean square (RMS) roughness values within proximity of each other (0.203–0.225 nm). On the other hand, films deposited from 1:1 (weight) blends with the conjugated polymer PBDB-T exhibited rougher surfaces (RMS = 2.35–2.38) with a fibrous appearance, likely as a result of the polymeric structure as previously noted.[72] Again, no obvious difference between NFA isomers could be identified.

Grazing-incidence wide-angle X-ray scattering (GIWAXS) of the same films was also carried out, to investigate the existence of ordered structures within the films. As shown in Fig. 2b, 2D diffractograms of films of pristine NFAs and polymer blends exhibited largely amorphous structures. The use of different isomers did not induce any noticeable change between film morphologies. Polymer blends gave rise to a peak at q = 2.95 nm^{-1}, which is assigned to the (100) lamellar stacking of the polymer.[72] This peak was enhanced upon annealing at 100 °C for 10 minutes, particularly in the *ortho* blend where the peak was absent prior to annealing (Fig. S4, ESI†). The amorphous morphology of pristine NFAs was further confirmed through differential scanning calorimetry (DSC), with an absence of thermal transitions between 25 and 280 °C in all materials, as depicted in Fig. S5 (ESI†).

Device performance

To test the suitability of our materials as electron acceptors in OPVs, devices were fabricated using an inverted architecture, as illustrated in Fig. 3a. The inverted architecture was based on ITO/ZnO/polymer:NFA/MoO$_x$/Ag, where PBDB-T was chosen as the electron donor polymer, given its well matched energy levels and success with similar materials in the past.[62,66]

The current–voltage (*J*–*V*) characteristics of devices under AM 1.5G illumination are shown in Fig. 3b, and device performance parameters are summarised in Table 3. It is clearly apparent that the choice of carborane isomer in the NFA has a

Table 3 Performance parameters of OPV devices

	V_{OC} (V)	J_{SC} (mA cm^{-2})	FF	PCE (%)
*p*Cb(T-IDIC)$_2$	0.93	5.36	0.39	1.93
*m*Cb(T-IDIC)$_2$	0.92	6.48	0.37	2.22
*o*Cb(T-IDIC)$_2$	0.95	7.40	0.43	3.00
*o*Cb(T-IDIC)$_2$-4F	0.92	10.27	0.54	5.07

major impact on device efficiency. Whilst devices made from *p*Cb(T-IDIC)$_2$ had an average PCE of 1.93%, and *m*Cb(T-IDIC)$_2$ had slightly higher 2.22%, *o*Cb(T-IDIC)$_2$ had considerably higher 3.00%. The performance of all three materials are in line with or higher than those previously reported for carborane-containing materials, verifying that molecular acceptors are a useful strategy in the synthesis of carborane-containing OPV materials.[40,41] Nevertheless, the overall performance of these materials remains modest compared to other non-carborane IDT-INCN flanked materials reported to date.[62–67] Although the open-circuit current (*V*$_{OC}$) values of the devices were high at around 0.93 V, the short-circuit current density (*J*$_{SC}$) remained relatively low, ranging from 5.36 to 7.40 mAcm^{-2}, and *J*–*V* curves exhibited non-ideal behaviours with fill factors between 37 and 43%.

High-performing OPVs require a sufficient energetic offset between donor and acceptor FMOs to promote exciton-to-charge separation, resulting in charge transfer from one material to the other. The energy diagram in Fig. 3c illustrates the offset between the reported LUMO of PBDB-T *versus p, m*, and *o*Cb(T-IDIC)$_2$, which allows for efficient exciton splitting.[73] Meanwhile, the offset between HOMOs is much narrower, with HOMOs of all three isomers being located around −5.39 eV. Increasing the offset by lowering the HOMO of the NFA is therefore a natural progression towards a higher *J*$_{SC}$.[74] Fluorination is an approach which has previously been used to lower the FMOs of similar IDT-INCN flanked A–D–A′–D–A materials, generally with great success in increasing *J*$_{SC}$.[62,66] With that in mind, we synthesised a fluorinated version of the highest performing isomer, namely *o*Cb(T-IDIC)$_2$-4F. As discussed in Section 2.2, this resulted in deeper energies of both the HOMO and the LUMO, resulting in larger energy offsets with respect to the polymer. This had the desired effect of increasing *J*$_{SC}$ from 7.40 to 10.27 mA cm^{-2}, and the corresponding EQE is shown in Fig. S6 (ESI†). It is possible that *J*$_{SC}$ could be improved further by combining donor and acceptor materials with a lesser spectral overlap (Fig. S7, ESI†).

In addition to increased *J*$_{SC}$, fluorination also improved the FF from 43 to 54%. To understand this change, charge carrier mobilities (*μ*) of the NFA blends were derived by the space charge limited current (SCLC) method.[75] *J*–*V* characteristics of single-carrier SCLC devices are depicted in Fig. S8 and S9 (ESI†) and mobilities are shown in Table S1 (ESI†). The hole mobilities of the blends are dominated by the p-type PBDB-T, with values in the order of 10^{-5} cm^2 V^{-1} s^{-1}. Meanwhile, electron-only SCLC devices revealed a much higher electron mobility of the blend with *o*Cb(T-IDIC)$_2$-4F at 6 × 10^{-7} cm^2 V^{-1} s^{-1}, compared to non-fluorinated NFAs in the
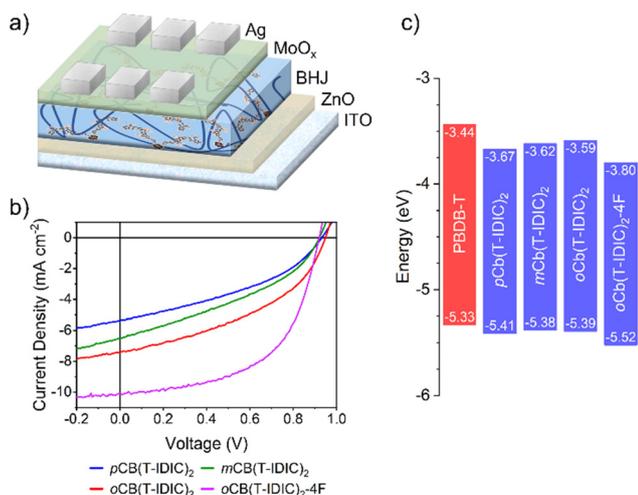

Fig. 3 (a) Illustration of the OPV device configuration (not to scale). (b) *J*–*V* curves of fabricated devices. (c) Energy diagram, comparing FMO levels of the donor polymer with the featured NFAs.

This journal is © The Royal Society of Chemistry 2023

J. Mater. Chem. C, 2023, **11**, 3989–3996 | **3993**

region $1–2 \times 10^{-7}$ cm^2 V^{-1} s^{-1}. This resulted in a more favourable μ_e/μ_h ratio and thus a higher FF.[76] As a consequence, the overall PCE was measured at 5.07% which, to the best of our knowledge, is the highest PCE reported for carborane-containing OPVs, and is more than double the best values previously reported.

Conclusions

In summary, we have synthesised four novel carborane-centred NFAs in an A–D–A′–D–A fashion. DFT calculations show that the carborane moieties do not participate in the π-conjugation, however, as HOMOs are located primarily on the IDT moieties, and LUMOs on the INCN moieties. Furthermore, we successfully fabricated OPV devices using PBDB-T:NFA blends, proving their applicability in OPV technology. The use of different carborane isomers (*para*, *meta*, and *ortho*) had a very limited effect on the optoelectronic properties of the materials, and no difference between isomers could be observed in thin-film morphology. On the other hand, the choice of isomer had a drastic impact on OPV performance, with the *ortho* isomer demonstrating superior device characteristics. To further increase the FMO offsets between the polymer donor and the NFA, a fluorinated version of the *ortho* isomer was synthesised. This increased the PCE from 3.00 to 5.07%, thus reporting the highest OPV efficiencies of carborane-containing OPV materials to date. Overall, our results demonstrate that carborane-containing materials can be utilised as electron acceptors in bulk heterojunction blends, and further highlight the viability of A–D–A′–D–A design strategies for such materials.

Author contributions

Filip Aniés (conceptualisation, investigation, project administration, visualisation, writing – original draft), Francesco Furlan (investigation, visualisation, writing – review & editing), Zhuoran Qiao (investigation, visualisation), Valentina Pirela (investigation, visualisation), Matthew Bidwell (investigation), Martina Rimmele (investigation), Jaime Martín (supervision), Nicola Gasparini (resources, supervision, writing – review & editing), Martin Heeney (conceptualisation, resources, supervision, writing – review & editing).

Conflicts of interest

There are no conflicts to declare.

Acknowledgements

Notes and references

1 R. N. Grimes, *Carboranes*, Academic Press, 3rd edn, 2016.

2 S.-Y. Lu and I. Hamerton, *Prog. Polym. Sci.*, 2002, **27**, 1661–1712.

3 R. Núñez, I. Romero, F. Teixidor and C. Viñas, *Chem. Soc. Rev.*, 2016, **45**, 5147–5173.

4 R. Núñez, M. Tarrés, A. Ferrer-Ugalde, F. F. de Biani and F. Teixidor, *Chem. Rev.*, 2016, **116**, 14307–14378.

5 Z. Chang, N. C. Okoye, M. J. Urffer, A. D. Green, K. E. Childs and L. F. Miller, *Nucl. Instrum. Methods Phys. Res., Sect. A*, 2015, **769**, 112–122.

6 D. Emin and T. L. Aselage, *J. Appl. Phys.*, 2005, **97**, 013529.

7 A. Pitto-Barry, *Polym. Chem.*, 2021, **12**, 2035–2044.

8 A. Marfavi, P. Kavianpour and L. M. Rendina, *Nat. Rev. Chem.*, 2022, **6**, 486–504.

9 P. Stockmann, M. Gozzi, R. Kuhnert, M. B. Sárosi and E. Hey-Hawkins, *Chem. Soc. Rev.*, 2019, **48**, 3497–3512.

10 J. Ochi, K. Tanaka and Y. Chujo, *Angew. Chem., Int. Ed.*, 2020, **59**, 9841–9855.

11 A. V. Marsh, N. J. Cheetham, M. Little, M. Dyson, A. J. P. White, P. Beavis, C. N. Warriner, A. C. Swain, P. N. Stavrinou and M. Heeney, *Angew. Chem., Int. Ed.*, 2018, **57**, 10640–10645.

12 A. V. Marsh, M. J. Dyson, N. J. Cheetham, M. Bidwell, M. Little, A. J. P. White, C. N. Warriner, A. C. Swain, I. McCulloch, P. N. Stavrinou, S. C. J. Meskers and M. Heeney, *Adv. Electron. Mater.*, 2020, **6**, 2000312.

13 A. V. Marsh, M. Little, N. J. Cheetham, M. J. Dyson, M. Bidwell, A. J. P. White, C. N. Warriner, A. C. Swain, I. McCulloch, P. N. Stavrinou and M. Heeney, *Chem. – Eur. J.*, 2021, **27**, 1970–1975.

14 K.-R. Wee, Y.-J. Cho, J. K. Song and S. O. Kang, *Angew. Chem., Int. Ed.*, 2013, **52**, 9682–9685.

15 H. Naito, K. Nishino, Y. Morisaki, K. Tanaka and Y. Chujo, *Angew. Chem., Int. Ed.*, 2017, **56**, 254–259.

16 K.-R. Wee, W.-S. Han, D. W. Cho, S. Kwon, C. Pac and S. O. Kang, *Angew. Chem., Int. Ed.*, 2012, **51**, 2677–2680.

17 K. Tanaka, M. Gon, S. Ito, J. Ochi and Y. Chujo, *Coord. Chem. Rev.*, 2022, **472**, 214779.

18 K. Kokado and Y. Chujo, *J. Org. Chem.*, 2011, **76**, 316–319.

19 M. Zhu, Q. Zhou, H. Cheng, Z. Meng, L. Xiang, Y. Sha, H. Yan and X. Li, *New J. Chem.*, 2022, **46**, 11382–11388.

20 H. Naito, Y. Morisaki and Y. Chujo, *Angew. Chem., Int. Ed.*, 2015, **54**, 5084–5087.

21 J. Li, C. Yang, X. Peng, Y. Chen, Q. Qi, X. Luo, W.-Y. Lai and W. Huang, *J. Mater. Chem. C*, 2018, **6**, 19–28.

22 Y. Cho, S. Kim, J. Lee, W. Han, C. H. Kim, H. Son and S. O. Kang, *Chem. – Eur. J.*, 2019, **25**, 8149–8156.

23 X. Wu, J. Guo, Y. Cao, J. Zhao, W. Jia, Y. Chen and D. Jia, *Chem. Sci.*, 2018, **9**, 5270–5277.

24 J. J. Peterson, A. R. Davis, M. Werre, E. B. Coughlin and K. R. Carter, *ACS Appl. Mater. Interfaces*, 2011, **3**, 1796–1799.

25 R. Huang, H. Liu, K. Liu, G. Wang, Q. Liu, Z. Wang, T. Liu, R. Miao, H. Peng and Y. Fang, *Anal. Chem.*, 2019, **91**, 14451–14457.

3994 | *J. Mater. Chem. C*, 2023, **11**, 3989–3996

This journal is © The Royal Society of Chemistry 2023

26 C. Li, M. P. Aldred, R. A. Harder, Y. Chen, D. S. Yufit, M.-Q. Zhu and M. A. Fox, *Chem. Commun.*, 2021, **57**, 9466–9469.

27 L. Böhling, A. Brockhinke, J. Kahlert, L. Weber, R. A. Harder, D. S. Yufit, J. A. K. Howard, J. A. H. MacBride and M. A. Fox, *Eur. J. Inorg. Chem.*, 2016, 403–412.

28 K.-R. Wee, Y.-J. Cho, S. Jeong, S. Kwon, J.-D. Lee, I.-H. Suh and S. O. Kang, *J. Am. Chem. Soc.*, 2012, **134**, 17982–17990.

29 R. Furue, T. Nishimoto, I. S. Park, J. Lee and T. Yasuda, *Angew. Chem., Int. Ed.*, 2016, **55**, 7171–7175.

30 A. R. Davis, J. J. Peterson and K. R. Carter, *ACS Macro Lett.*, 2012, **1**, 469–472.

31 Y. Kim, S. Park, Y. H. Lee, J. Jung, S. Yoo and M. H. Lee, *Inorg. Chem.*, 2016, **55**, 909–917.

32 Q. Li, C. Shi, M. Huang, X. Zhang, F. Sun, Y. Zheng, H. Yan, C. Yang and A. Yuan, *Dalton Trans.*, 2021, **50**, 16304–16310.

33 K. Kokado and Y. Chujo, *Macromolecules*, 2009, **42**, 1418–1420.

34 K. Kokado, Y. Tokoro and Y. Chujo, *Macromolecules*, 2009, **42**, 9238–9242.

35 M. Tominaga, Y. Morisaki, H. Naito and Y. Chujo, *Polym. J.*, 2014, **46**, 740–744.

36 K. Kokado, Y. Tokoro and Y. Chujo, *Macromolecules*, 2009, **42**, 2925–2930.

37 K. Kokado, M. Tominaga and Y. Chujo, *Macromol. Rapid Commun.*, 2010, **31**, 1389–1394.

38 J. Marshall, Z. Fei, C. P. Yau, N. Yaacobi-Gross, S. Rossbauer, T. D. Anthopoulos, S. E. Watkins, P. Beavis and M. Heeney, *J. Mater. Chem. C*, 2014, **2**, 232–239.

39 J. Marshall, B. C. Schroeder, H. Bronstein, I. Meager, S. Rossbauer, N. Yaacobi-Gross, E. Buchaca-Domingo, T. D. Anthopoulos, N. Stingelin, P. Beavis and M. Heeney, *Macromolecules*, 2014, **47**, 89–96.

40 J. Marshall, J. Hooton, Y. Han, A. Creamer, R. S. Ashraf, Y. Porte, T. D. Anthopoulos, P. N. Stavrinou, M. A. McLachlan, H. Bronstein, P. Beavis and M. Heeney, *Polym. Chem.*, 2014, **5**, 6190–6199.

41 F. Aniés, Z. Qiao, M. I. Nugraha, A. Basu, T. D. Anthopoulos, N. Gasparini and M. Heeney, *Polymer*, 2022, **240**, 124481.

42 B. Fabre, S. Chayer and M. G. H. Vicente, *Electrochem. Commun.*, 2003, **5**, 431–434.

43 Y. C. Simon, J. J. Peterson, C. Mangold, K. R. Carter and E. B. Coughlin, *Macromolecules*, 2009, **42**, 512–516.

44 I. Nar, A. Atsay, A. Altındal and E. Hamuryudan, *Inorg. Chem.*, 2018, **57**, 2199–2208.

45 F. Ye, S. Zhang, J. Warby, J. Wu, E. Gutierrez-Partida, F. Lang, S. Shah, E. Saglamkaya, B. Sun, F. Zu, S. Shoaee, H. Wang, B. Stiller, D. Neher, W.-H. Zhu, M. Stolterfoht and Y. Wu, *Nat. Commun.*, 2022, **13**, 7454.

46 B. G. Kim, W. Jang, H. Jeon, S. Lee, W.-S. Han and D. H. Wang, *Sol. Energy Mater. Sol. Cells*, 2020, **208**, 110414.

47 A. M. Spokoyny, T. C. Li, O. K. Farha, C. W. Machan, C. She, C. L. Stern, T. J. Marks, J. T. Hupp and C. A. Mirkin, *Angew. Chem., Int. Ed.*, 2010, **49**, 5339–5343.

48 T. C. Li, A. M. Spokoyny, C. She, O. K. Farha, C. A. Mirkin, T. J. Marks and J. T. Hupp, *J. Am. Chem. Soc.*, 2010, **132**, 4580–4582.

49 S. Şener, *Heterocycl. Commun.*, 2020, **26**, 37–45.

50 Q. He, P. Kafourou, X. Hu and M. Heeney, *SN Appl. Sci.*, 2022, **4**, 247.

51 A. Wadsworth, M. Moser, A. Marks, M. S. Little, N. Gasparini, C. J. Brabec, D. Baran and I. McCulloch, *Chem. Soc. Rev.*, 2019, **48**, 1596–1625.

52 G. Zhang, F. R. Lin, F. Qi, T. Heumüller, A. Distler, H.-J. Egelhaaf, N. Li, P. C. Y. Chow, C. J. Brabec, A. K.-Y. Jen and H.-L. Yip, *Chem. Rev.*, 2022, **122**, 14180–14274.

53 Z. Zhang, J. Yuan, Q. Wei and Y. Zou, *Front. Chem.*, 2018, **6**, 414.

54 G. Zhang, J. Zhao, P. C. Y. Chow, K. Jiang, J. Zhang, Z. Zhu, J. Zhang, F. Huang and H. Yan, *Chem. Rev.*, 2018, **118**, 3447–3507.

55 W. Zhang, J. Smith, S. E. Watkins, R. Gysel, M. McGehee, A. Salleo, J. Kirkpatrick, S. Ashraf, T. Anthopoulos, M. Heeney and I. McCulloch, *J. Am. Chem. Soc.*, 2010, **132**, 11437–11439.

56 S. Holliday, R. S. Ashraf, A. Wadsworth, D. Baran, S. A. Yousaf, C. B. Nielsen, C.-H. Tan, S. D. Dimitrov, Z. Shang, N. Gasparini, M. Alamoudi, F. Laquai, C. J. Brabec, A. Salleo, J. R. Durrant and I. McCulloch, *Nat. Commun.*, 2016, **7**, 11585.

57 Z. Fei, F. D. Eisner, X. Jiao, M. Azzouzi, J. A. Röhr, Y. Han, M. Shahid, A. S. R. Chesman, C. D. Easton, C. R. McNeill, T. D. Anthopoulos, J. Nelson and M. Heeney, *Adv. Mater.*, 2018, **30**, 1705209.

58 Y. Lin, Q. He, F. Zhao, L. Huo, J. Mai, X. Lu, C.-J. Su, T. Li, J. Wang, J. Zhu, Y. Sun, C. Wang and X. Zhan, *J. Am. Chem. Soc.*, 2016, **138**, 2973–2976.

59 Y. Lin, J. Wang, Z.-G. Zhang, H. Bai, Y. Li, D. Zhu and X. Zhan, *Adv. Mater.*, 2015, **27**, 1170–1174.

60 Y. Wu, H. Bai, Z. Wang, P. Cheng, S. Zhu, Y. Wang, W. Ma and X. Zhan, *Energy Environ. Sci.*, 2015, **8**, 3215–3221.

61 Y. Lin, Z.-G. Zhang, H. Bai, J. Wang, Y. Yao, Y. Li, D. Zhu and X. Zhan, *Energy Environ. Sci.*, 2015, **8**, 610–616.

62 H. S. Kim, S. Rasool, W. S. Shin, C. E. Song and D.-H. Hwang, *ACS Appl. Mater. Interfaces*, 2020, **12**, 50638–50647.

63 X. Chen, Y. Luo, M. Lv, C. Yi, M. Yin, S. Liu, Z. Xiao and L. Ding, *Mater. Chem. Front.*, 2022, **6**, 802–806.

64 G. Cai, Z. Chen, M. Li, Y. Li, P. Xue, Q. Cao, W. Chi, H. Liu, X. Xia, Q. An, Z. Tang, H. Zhu, X. Zhan and X. Lu, *Adv. Sci.*, 2022, **9**, 2103428.

65 M. J. Cho, G. E. Park, S. Y. Park, Y.-U. Kim and D. H. Choi, *RSC Adv.*, 2017, **7**, 38773–38779.

66 J. Zhu, X. Zheng, H. Tan, H. Tan, J. Yang, J. Yu and W. Zhu, *Chem. Phys. Lett.*, 2019, **726**, 7–12.

67 F. Zhang, X. Yu, M. Xiong, Z. Yin, Y. Wang, J. Yu, J. Cao, H. Tan and M. Zhang, *Synth. Met.*, 2021, **278**, 116838.

68 D. F. Zeigler, K.-S. Chen, H.-L. Yip, Y. Zhang and A. K.-Y. Jen, *J. Polym. Sci., Part A: Polym. Chem.*, 2012, **50**, 1362–1373.

69 H. Yamamoto, J. Ochi, K. Yuhara, K. Tanaka and Y. Chujo, *Cell Rep. Phys. Sci.*, 2022, **3**, 100758.

70 S. Kwon, K.-R. Wee, Y.-J. Cho and S. O. Kang, *Chem. – Eur. J.*, 2014, **20**, 5953–5960.

This journal is © The Royal Society of Chemistry 2023

J. Mater. Chem. C, 2023, **11**, 3989–3996 | **3995**

71 J. Sworakowski, J. Lipiński and K. Janus, *Org. Electron.*, 2016, **33**, 300–310.

72 D. Qian, L. Ye, M. Zhang, Y. Liang, L. Li, Y. Huang, X. Guo, S. Zhang, Z. Tan and J. Hou, *Macromolecules*, 2012, **45**, 9611–9617.

73 J. Bertrandie, J. Han, C. S. P. De Castro, E. Yengel, J. Gorenflot, T. Anthopoulos, F. Laquai, A. Sharma and D. Baran, *Adv. Mater.*, 2022, 2202575.

74 S. Karuthedath, J. Gorenflot, Y. Firdaus, N. Chaturvedi, C. S. P. De Castro, G. T. Harrison, J. I. Khan, A. Markina, A. H. Balawi, T. A. Dela Peña, W. Liu, R.-Z. Liang, A. Sharma, S. H. K. Paleti, W. Zhang, Y. Lin, E. Alarousu, S. Lopatin, D. H. Anjum, P. M. Beaujuge, S. De Wolf, I. McCulloch, T. D. Anthopoulos, D. Baran, D. Andrienko and F. Laquai, *Nat. Mater.*, 2021, **20**, 378–384.

75 P. W. M. Blom, M. J. M. de Jong and M. G. van Munster, *Phys. Rev. B: Condens. Matter Mater. Phys.*, 1997, **55**, R656–R659.

76 L. J. A. Koster, V. D. Mihailetchi and P. W. M. Blom, *Appl. Phys. Lett.*, 2006, **88**, 052104.

3996 | *J. Mater. Chem. C*, 2023, **11**, 3989–3996

This journal is © The Royal Society of Chemistry 2023